

Does the Narrow [O III] $\lambda 5007$ Line Reflect the Stellar Velocity Dispersion in AGN?

Todd A. Boroson

National Optical Astronomy Observatory, P.O. Box 26732, Tucson, AZ 85726-6732

tboroson@noao.edu

ABSTRACT

It has been proposed that the width of the narrow [O III] $\lambda 5007$ emission line can be used as a surrogate for the stellar velocity dispersion in active galaxies. This proposition is tested using the SDSS EDR spectra of 107 low-redshift radio-quiet QSOs and Seyfert 1 galaxies by investigating the correlation between black hole mass, as determined from $H\beta$ FWHM and optical luminosity, and [O III] FWHM. The correlation is real, but the scatter is large. Without additional information or selection criteria, the [O III] width can predict the black hole mass to a factor of 5.

Subject headings: galaxies: active, bulges—quasars: emission lines

1. Introduction

The correlation of nuclear black hole mass M_\bullet and bulge stellar velocity dispersion σ_* is now well established in nearby galaxies (Tremaine et al. 2002). The possibility of extending the study of this relationship to active galaxies, using diagnostics that can be easily measured even at substantial redshifts, has been explored as a result of two techniques: (1) the use of reverberation mapping to calibrate a relation between luminosity and radius of the broad line region (BLR), and (2) the use of the narrow [O III] $\lambda 5007$ emission line width as a surrogate for stellar velocity dispersion.

If the BLR is in virial equilibrium, the mass of the central black hole is given by $M_\bullet = v^2 R_{\text{BLR}}/G$, where v and R_{BLR} are the characteristic velocity and radius of the BLR. Scale factors for converting measured quantities to truly representative and corresponding velocities and radii depend on the unknown kinematic structure of the BLR. However, several studies have shown that estimates of the black hole mass that are consistent with other methods can be derived in this way. Gebhardt et al. (2000) and Merritt and Ferrarese

(2000) show that black hole masses derived using velocities from the $H\beta$ line width and radii from reverberation mapping time lags fall on the same relation in the M_\bullet vs σ_* diagram as those derived from spatially resolved spectroscopy. Admittedly, this confirmation is possible for only a small number of objects, but the scatter appears consistent with measurement errors. Kaspi et al. (2000) showed that a good correlation exists between BLR radius and the monochromatic luminosity L_{5100} with a power law index of 0.7 for their sample of reverberation-mapped AGNs, allowing this easily measured luminosity to be substituted for time lags derived from arduous monitoring campaigns. This set of correlations (the "photoionization method" (Wandel, Peterson, and Malkan 1999)) has already been used in a number of studies of black hole masses in AGNs including Merritt and Ferrarese (2000), Laor (2000), Lacy et al. (2001), Shields et al. (2002), Vestergaard (2002), Oshlack et al. (2002), and Jarvis and McLure (2002).

The evidence that the [O III] line width in QSOs is dominated by the gravitational potential on the scale of the host galaxy bulge is primarily the result of two studies. Nelson and Whittle (1996) studied the relationship between the widths of narrow emission lines and near-nuclear stellar velocity dispersion for a sample of 75 Seyfert galaxies. They found a moderately strong correlation between [O III] FWHM and σ_* ($r = 0.48$, $P(\text{null}) = 0.0038\%$ for 66 objects) with a slope flatter than unity due to anomalously broad [O III] lines in objects that have powerful linear radio sources. As a consequence of this finding, Nelson (2000) proposed that the [O III] FWHM could be used to extend the M_\bullet vs σ_* relation to AGNs. His study compared the location of 20 Seyfert galaxies and 12 QSOs in the M_\bullet vs [O III] FWHM plane with the M_\bullet vs σ_* relation from Gebhardt et al. (2000) (where $\text{FWHM} = 2.35 \times \sigma$). The data in his study were gathered from a number of sources in the literature, and comprised all objects for which M_\bullet values had been derived from reverberation mapping measurements. Nelson (2000) found that for these AGN, the M_\bullet and [O III] FWHM values were strongly correlated and consistent with the Gebhardt et al. (2000) relation, though with substantial scatter.

Because of the scatter seen by Nelson (2000) in the M_\bullet vs [O III] FWHM relation and the heterogeneous data used in that study, it is useful to further investigate that relation. If the relation is tight, it provides a mechanism for studying the evolution of the relationship between black hole and galaxy formation processes, as the emission lines, $H\beta$ and [O III] $\lambda 5007$ can be easily observed and measured to substantial redshifts. An initial attempt to compare this relationship between low and high redshift sample using data from the literature has been published by Shields et al. (2002).

This paper reports on an investigation of the M_\bullet vs [O III] FWHM relation for AGN from a large, homogeneous data set, the Sloan Digital Sky Survey (SDSS) Early Data Release

(EDR) spectra. The goal of this study is to establish the reality of this relation, measure its scatter, and detect any selection effects that would compromise a comparison of low and high redshift samples.

2. The Sample

The QSOs included in the sample were all drawn from the SDSS EDR (Stoughton et al. 2002). The SDSS ought to provide an excellent dataset for this purpose, as it has uniform photometry and spectroscopy, and sufficient spectral resolution ($R \sim 1800$) to resolve the [O III] line (York et al. 2000). Although Schneider et al. (2002) have generated an EDR Quasar catalog, it has a luminosity constraint ($M_I \leq -23$) and a line width constraint ($\text{FWHM} \geq 1000 \text{ km s}^{-1}$). Since the current study wants the largest possible range of M_{\bullet} , which depends on both luminosity and line width, a new catalog was generated from the SDSS database.

First, spectra of all QSO candidates, having g^* magnitudes brighter than 18.0 and redshifts less than 0.5 were downloaded from the archive. The magnitude limit was imposed because it was recognized that the fainter objects would not have spectra with sufficient signal-to-noise to support the analysis. The redshift limit was imposed to ensure the the H β and [O III] lines would be in a region free of noise from strong night-sky emission lines. This initial list contained 201 objects. Visual inspection of these spectra showed that further trimming of the list would be required to remove those objects that were too low in signal-to-noise or which had no obvious broad line region. This resulted in a list of 121 objects. Two entries in this list are actually two independent observations of the same object, SDSS J032205.05+001201.4

Each spectrum was shifted to a rest wavelength scale, using the redshift obtained from the SDSS database, and rebinned to a common format with 1.5\AA pixel^{-1} . The complex Fe II emission was then measured and subtracted using the technique and template described in Boroson and Green (1992) (BG92). Briefly, a template with strong, narrow Fe II emission was constructed from a spectrum of the low redshift QSO I Zwicky 1. Lines attributed to other ions were removed and the continuum subtracted. This template was then broadened and multiplied by scaling factors and subtracted from each QSO spectrum. Different combinations of broadening and scaling were tried until the continuum on either side of the H β -[O III] complex appeared flat and featureless. In practice, the initial guess for broadening was obtained by measuring the H β width from the spectrum and assuming that the Fe II width was identical. This produced a satisfactory result in almost all cases.

Once the best Fe II broadening and scaling were identified, a Fe II-subtracted spectrum was generated and the continuum was fit and removed between the emission lines over the range $\lambda\lambda 4200 - 6000$. $H\beta$ and $\lambda 5007$ widths were measured from these normalized spectra. These widths are not derived from fits to functions, but are actual measured widths of the two lines at half of their maximum intensity. Six of the objects had no detectable (or very weak) [O III] emission, and so they were removed from the sample. The remaining 115 objects, together with $H\beta$ FWHM and $\sigma_{[OIII]}$ (FWHM/2.35; corrected for instrumental resolution; see below) are listed in table 1. Note that the two sets of measurements for the object observed (and analyzed) twice, SDSS J032205.05+001201.4, differ by 5% or less.

In the case of the [O III] widths, the instrumental resolution, 166 km s^{-1} (or 2.8A at $\lambda 5007$), has been subtracted in quadrature from the measured widths. Note that this correction only changes the line width by as much as 20% in 12 of the 115 objects.

For the $H\beta$ line widths an additional caveat is required. In approximately one-fourth of the spectra, a narrow $H\beta$ spike is seen on top of the broad $H\beta$ line. We have ignored this spike in measuring the FWHM of the $H\beta$ line. Although such spikes include only a small fraction of the flux in the line, they can dramatically change the FWHM value measured.

Recently Vestergaard (2002) has discussed at length the correct method for measuring the BLR line width for the calculation of M_\bullet . As she points out, the appropriate BLR velocity dispersion is that measured from the ‘rms’ spectrum, which represents the varying part of the line profile. She goes on to compare the FWHM $H\beta$ values from the rms spectra of Kaspi et al. (2000) with mean and single-epoch measurements of the same objects. She concludes that, in general, the best way to substitute a single-epoch spectrum for the rms spectrum is to remove the Fe II emission, but leave the narrow component of $H\beta$ to be included in the measurement. The conclusion that the narrow component should not be removed is motivated primarily by the single object PG1704+608 (3C 351), which has a strong, narrow spike on top of a very broad $H\beta$ line. Measurements of the width of the broad lines in this object include 6560 km s^{-1} ($H\beta$; BG92), $13,000 \text{ km s}^{-1}$ ($H\alpha$; Eracleous and Halpern (1994)), $10,000 \text{ km s}^{-1}$ ($H\beta$; Netzer et al. (1982)). However, Kaspi et al. (2000) quote 890 km s^{-1} for the mean spectrum and 400 km s^{-1} for the rms spectrum. Is it really the narrow component of $H\beta$ that is varying?

There are several reasons to think that the idea that it is the narrow part of the line varying is in error. First, the narrow component only accounts for a small fraction of the line flux – around 10% in this object. Thus, to produce a change in total line flux of a factor of two, as is seen in the Kaspi et al. (2000) data, it would need to vary by a factor of 20. This is inconsistent with published spectra in Kaspi et al. (2000) and BG92, and the SDSS EDR spectrum of this object, all of which show the narrow $H\beta$ at similar strength relative

to the [O III] lines. Second, the adoption of such a small characteristic velocity width for the BLR results in a very low black hole mass. The Kaspi et al. (2000) value based on the rms spectrum is $7.5 \times 10^6 M_\odot$. The black hole mass based on the BG92 line width is $2.0 \times 10^9 M_\odot$. The small black hole mass would imply an unreasonably small Eddington luminosity, resulting in an Eddington ratio of 30, while the high black hole mass gives a more sensible Eddington ratio of 0.1. Finally, we note that a drawback of the use of the rms spectrum to identify the changing part of the line is that variations in line profiles due to seeing differences or instrumental differences from observation to observation will cause residuals (see footnote 9 in Kaspi et al. (2000)). The rms spectrum of PG 1704+608 shows significant residual emission at the [O III] lines, ten times as strong as the narrow H β spike in that spectrum (Kaspi 2002). This suggests that in this object, the rms spectrum is misleading as an indicator of what part of the H β line is varying as a response to continuum variations.

Table 1 also lists for each object the black hole mass, derived using the formula $M_\bullet = v^2 R_{\text{BLR}}/G$, where $v = \sqrt{3}/2 \text{FWHM}_{H\beta}$, and $R_{\text{BLR}} = 32.9(\lambda L_{5100}/10^{44} \text{ergs s}^{-1})^{0.7}$ light days (Kaspi et al. 2000). The values of L_{5100} were derived from the r^* photometry in the SDSS database. Fluxes were converted to luminosities using the Schlegel et al. (1998) maps for correcting for galactic absorption, $H_0 = 75 \text{ km s}^{-1} \text{ Mpc}^{-1}$, and $q_0 = 0.5$.

Finally, Table 1 also lists $\log R$, a measure of radio loudness. The FIRST catalog (Becker, White, and Helfand 1995) and the NVSS catalog (Condon et al. 1998) were searched at the position of each object. All but one of the objects, SDSS J173348.81+585651.0, are in regions covered by one or the other radio survey. Any source within 30 arcseconds was declared a match, though we note that the positional accuracy of all these surveys is good enough that a match with a radio core ought to lie within 2 arcseconds. Thus, we flag those that have differences between the radio and optical centroid of more than 2 arcseconds with a colon in Table 1. R is the ratio of flux density at 5 GHz to flux density at $\lambda 2500$. In computing this, a spectral slope of -0.3 was used to transform the total observed radio flux density at 1.4 GHz, and an optical spectral slope of -1.0 was used to transform the g^* magnitude.

Figure 1 shows the black hole mass plotted against the [O III] line width for the 115 SDSS low-redshift QSOs. The seven objects with $\log R > 1$, the usual criterion for radio-loud, are plotted as open circles. The one object unobserved in the radio is plotted as an open triangle. The remaining 107 objects are plotted as solid squares.

3. Discussion

A correlation between M_{\bullet} and [O III] width is evident in Figure 1, though the scatter is large. For the following fitting and statistical analysis the two observations of SDSS J032205.05+001201.4 have been combined by averaging their measurements and the radio-loud objects have been removed, resulting in a sample of 107 objects. The correlation coefficient is $r = 0.44$ ($P = 6 \times 10^{-6}$) for the 107 objects that are not radio-loud. Two lines through the points are shown in Figure 1. The solid line is a fit to the radio-quiet points, using the least-squares bisector (Isobe et al. 1990), which is plausible for situations where both variables have large uncertainties. This is the same type of fit used by Nelson (2000). For an equation of the form $\log(M_{\bullet}/M_{\odot}) = \alpha + \beta \log(\sigma/\sigma_0)$, the fit has coefficients $\alpha = 8.05 \pm 0.07$ and $\beta = 3.59 \pm 0.47$ where $\sigma_0 = 200 \text{ km s}^{-1}$. The dashed line is that derived by Tremaine et al. (2002) who find $\alpha = 8.13 \pm 0.06$ and $\beta = 4.02 \pm 0.32$ from a sample of 31 nearby galaxies. For comparison, the sample of Nelson (2000), analyzed in the same way has an identical correlation coefficient of $r = 0.44$, and coefficients of $\alpha = 6.54$ and $\beta = 3.50$ for the 28 radio-quiet objects.

One measure of the scatter is the standard deviation of the points from the bisector fit in $\log M_{\bullet}$. This is the accuracy with which $\sigma_{[\text{OIII}]}$ could be used to calculate M_{\bullet} . For the 107 radio-quiet low-redshift objects, the standard deviation is 0.67 in $\log M_{\bullet}$, or a factor of a little less than 5. Alternatively, one can compare the fit to the data with the Tremaine et al. (2002) line, which represents the relationship that we believe we are modeling. Clearly, both the slope and intercept (at $\sigma_0 = 200 \text{ km s}^{-1}$) are consistent between the two fits. This is interesting not only as confirmation that the two approaches are demonstrating the same physical relationship, but also because the scatter of the AGN points around the non-AGN fit is close to symmetric.

The fact that the scatter is larger than the non-AGN sample (Tremaine et al. (2002) quote intrinsic dispersion in $\log M_{\bullet}$ of 0.3 or less) is not surprising. The scatter is not primarily due to measurement errors, as these are probably no more than about 10% for the line widths and a few percent for the magnitudes. However, both $\text{H}\beta$ FWHM and optical brightness vary in most AGNs, and these will produce errors in M_{\bullet} . In addition, luminosity is being used to predict R_{BLR} , and this relation has significant scatter (Kaspi et al. 2000). On the abscissa, [O III] FWHM is not a perfect predictor of stellar velocity dispersion (Nelson and Whittle 1996), but shows scatter of about 0.2 in the log around a ratio of unity. Nelson and Whittle (1996) explored this relationship in detail, and found that several properties indicated high [O III] widths relative to the stellar velocity dispersion, including powerful linear radio sources and systems showing obvious signs of interaction. We have removed the radio-loud objects in this study, but have no way of filtering by properties such as host

galaxy interaction. The fact that the scatter is approximately equal on the two sides of the Tremaine et al. (2002) fit suggests that the explanation is not as simple as objects with anomalously high [O III] widths.

Given that one goal of this study is to lay the groundwork for an exploration of the M_{\bullet} vs σ_* relationship as a function of redshift, it is worthwhile to investigate the extent to which the fit depends on the luminosity range of the sample. The 107 low redshift radio-quiet objects were divided into two sub-samples of equal size, one with $L_{5100} < 2.7 \times 10^{44}$ ergs s^{-1} and one with $L_{5100} > 2.7 \times 10^{44}$ ergs s^{-1} . Figure 2 shows these two sub-samples plotted with different symbols and the bisector fits to the sub-samples. The coefficients of the fits are $\alpha = 8.02$ and $\beta = 2.48 \pm 0.72$ for the low luminosity objects and $\alpha = 8.28$ and $\beta = 1.81 \pm 0.52$ for the high luminosity objects. Thus, there is a tendency for the slope to flatten in samples restricted to a smaller range of luminosity, particularly for high luminosity. This is not surprising in that the dependence of M_{\bullet} on luminosity results in a dividing line between low and high luminosity samples that is flatter than the relation itself. This, combined with the large scatter, results in a flatter fit. For comparison with other samples, it certainly seems advisable to maintain the largest possible range of luminosity.

I am grateful to Mike Brotherton and Richard Green for helpful conversations.

Funding for the creation and distribution of the SDSS Archive has been provided by the Alfred P. Sloan Foundation, the Participating Institutions, the National Aeronautics and Space Administration, the National Science Foundation, the U.S. Department of Energy, the Japanese Monbukagakusho, and the Max Planck Society. The SDSS Web site is <http://www.sdss.org/>.

This research has made use of the NASA/IPAC Extragalactic Database (NED) which is operated by the Jet Propulsion Laboratory, California Institute of Technology, under contract with the National Aeronautics and Space Administration.

REFERENCES

Becker, R.H., White, R.L., and Helfand, D., J. 1995, ApJ, 450, 559

Boroson, T.A. and Green, R.F. 1992, ApJS, 80, 109

Condon, J.J., Cotton, W.D., Greisen, E.W., Yin, Q.F., Perley, R.A., Taylor, G.B., Broderick, J.J. 1998, AJ, 115, 1693

Eracleous, M. and Halpern, J. P. 1994, ApJS, 90, 1

Gebhardt, K. et al. 2000, *ApJ*, 543, L5

Isobe, T., Feigelson, E.D., Akritas, M.G., and Babu, G.J. 1990, *ApJ*, 364, 104

Jarvis, M. J. and McLure, R. J. 2002, *MNRAS*, 336, L38

Kaspi, S. 2002, private communication

Kaspi, S., Smith, P.S., Netzer, H., Maoz, D., Jannuzi, B., and Giveon, U. 2000, *ApJ*, 533, 631

Lacy, M., Laurent-Muehleisen, S. A., Ridgway, S. E., Becker, R. H., and White, R. L. 2001, *ApJ*, 551, L17

Laor, A. 2000, *ApJ*, 543, L111

Merritt, D. and Ferrarese, L. 2000, in *ASP Conf. Ser.* 249, The Central kpc of Starbursts and AGN, ed. J. H. Knapen, J. E. Beckman, I. Schlosman, and T. J. Mahoney (San Francisco: ASP), 335

Nelson, C.H. 2000, *ApJ*, 544, L91

Nelson, C.H. and Whittle, M. 1986, *ApJ*, 465, 96

Netzer, H., Wills, B.J., and Wills, D. 1982, *ApJ*, 254, 489

Oshlack, A.Y.K.N., Webster, R. L., and Whiting, M. T. 2002, *ApJ*, 576, 81

Schlegel, D.J., Finkbeiner, D.P., and Davis, M. 1998, *ApJ*, 500, 525

Schneider, D. P., et al. *AJ*, 123, 567

Shields, G.A., Gebhardt, K., Salviander, S., Wills, B.J., Xie, B., Brotherton, M.S., Yuan, J., and Dietrich, M., 2002, *ApJ*, in press

Stoughton, C., Lupton, R.H., Bernardi, M., et al. 2002, *AJ*, 123, 485

Tremaine, S., Gebhardt, K., Bender, R., Bower, G., Dressler, A., Faber, S.M., Filippenko, A.V., Green, R., Grillmair, C., Ho, L.C., Kormendy, J., Lauer, T.R., Magorrian, J., Pinkney, J., and Richstone, D. 2002, *ApJ*, 574, 740

Vestergaard, M. 2002, *ApJ*, 571, 733

Wandel, A., Peterson, B.M., and Malkan, M.A. 1999, *ApJ*, 526, 579

York, D.G., Adelman, J., Anderson, J.E., et al. 2000, AJ, 120, 1579

Table 1. Line Widths and Black Hole Masses of SDSS Sample

SDSS J	z	FWHM _{Hβ} km s $^{-1}$	$\sigma_{\text{[OIII]}}$ km s $^{-1}$	$\log M_{\bullet}$ M_{\odot}	$\log R$
000011.97+000225.1	0.4790	2290	290	8.17	not detected
000710.02+005329.0	0.3164	11158	271	9.56	0.27
001327.31+005232.0	0.3626	1549	183	7.71	not detected
001903.17+000659.1	0.0726	3283	90	8.10	not detected
002444.11+003221.4	0.4004	9159	180	9.56	1.42:
003238.20–010035.3	0.0919	1919	73	7.10	not detected
003431.74–001312.7	0.3811	1197	223	7.39	not detected
003723.50+000812.6	0.2518	2598	196	7.85	not detected
003847.98+003457.5	0.0806	7141	161	8.33	0.65
010342.73+002537.3	0.3938	2123	180	8.07	not detected
010939.02+005950.4	0.0929	2765	144	7.63	0.29
011254.92+000313.0	0.2385	3135	177	8.04	not detected
011448.68–002946.1	0.0338	3450	109	7.61	0.62:
011703.58+000027.4	0.0456	2685	136	7.57	-0.36
011929.06–000839.8	0.0901	666	202	6.17	not detected
012159.82–010224.5	0.0544	4097	194	7.97	0.26
013418.19+001536.7	0.3989	4085	290	8.85	not detected
013521.68–004402.1	0.0984	1555	290	7.21	0.44
013527.85–004447.9	0.0805	3314	124	7.93	not detected
014017.07–005003.0	0.3346	4789	164	8.98	not detected
014238.48+000514.7	0.1458	2783	121	7.68	not detected
014644.82–004043.1	0.0827	969	87	6.80	0.54
015910.06+010514.5	0.2174	3326	269	8.15	not detected
015950.24+002340.9	0.1626	1956	292	7.91	1.04
020615.99–001729.2	0.0427	6887	169	8.45	0.06
021359.79+004226.8	0.1821	4592	207	8.28	0.97
023335.38–010744.7	0.3679	2444	247	8.00	not detected
024651.91–005931.0	0.4681	1426	77	7.96	0.41:
025007.03+002525.4	0.1977	2086	112	7.56	not detected
025505.67+002523.0	0.3541	4715	229	8.63	not detected

Table 1—Continued

SDSS J	z	FWHM _{Hβ} km s $^{-1}$	$\sigma_{\text{[OIII]}}$ km s $^{-1}$	$\log M_{\bullet}$ M_{\odot}	$\log R$
025646.97+011349.4	0.1766	2512	226	7.73	not detected
030124.26+011022.9	0.0715	3073	183	7.57	not detected
030144.20+011530.9	0.0747	4221	215	7.93	not detected
030417.78+002827.3	0.0445	1173	94	6.58	not detected
030639.58+000343.1	0.1073	2567	196	7.75	0.66
031027.83–004950.8	0.0804	3073	66	7.75	not detected
031427.47–011152.4	0.3869	1660	188	7.77	not detected
032205.05+001201.4	0.4719	3604	247	8.76	not detected
032205.05+001201.4	0.4717	3789	255	8.80	not detected
032213.90+005513.5	0.1851	2339	118	8.06	not detected
032337.65+003555.6	0.2154	1395	194	7.28	not detected
032559.97+000800.7	0.3606	12380	175	9.57	not detected
032729.89–005958.4	0.1340	6381	164	8.61	not detected
034226.50–000427.1	0.3762	2573	239	8.18	not detected
101044.51+004331.2	0.1780	6221	177	8.85	-0.29
101314.87–005233.6	0.2759	1506	368	7.44	not detected
102448.57+003537.9	0.0954	1481	90	7.04	not detected
102936.10–010201.0	0.1398	5894	199	8.35	not detected
103457.29–010209.1	0.3280	1216	124	7.40	not detected
104230.14+010223.7	0.1155	673	166	6.53	not detected
104332.88+010108.9	0.0719	2499	109	7.55	not detected
105706.94–004145.1	0.1876	1784	169	7.50	not detected
110057.71–005304.6	0.3776	4851	166	8.71	not detected
105935.76–000551.3	0.2825	2296	150	7.82	not detected
113541.21+002235.3	0.1753	994	103	6.88	not detected
113909.66–001608.7	0.1351	3598	115	7.79	not detected
114335.37–002942.4	0.1715	7048	115	8.54	not detected
113909.66–001608.7	0.1351	3752	97	7.83	not detected
113923.66+002301.6	0.4721	15559	329	9.92	not detected
115235.00–000542.7	0.1288	3894	90	7.81	not detected

Table 1—Continued

SDSS J	z	FWHM _{Hβ} km s $^{-1}$	$\sigma_{\text{[OIII]}}$ km s $^{-1}$	$\log M_{\bullet}$ M_{\odot}	log R
115758.73–002220.9	0.2598	4635	141	8.65	not detected
120014.08–004638.7	0.1793	2290	161	7.62	1.80:
122432.41–002731.5	0.1571	1160	136	6.85	not detected
124324.22+010028.1	0.0897	5604	121	8.02	not detected
124623.00+002839.9	0.0884	2518	115	7.40	0.78
130023.22–005429.8	0.1222	839	118	6.45	not detected
130713.25–003601.7	0.1700	1537	158	7.28	not detected
130756.58+010709.6	0.2754	3913	290	8.43	not detected
131108.48+003151.8	0.4293	1401	242	7.61	not detected
132135.33–001305.8	0.0822	4289	147	8.04	0.34
134044.52–004516.7	0.3844	3215	292	8.42	not detected
134113.94–005315.0	0.2373	2030	239	7.67	1.17
134251.61–005345.4	0.3259	3166	492	8.43	not detected
134351.07+000434.7	0.0736	1672	87	6.87	not detected
134452.91+000520.2	0.0871	2000	166	7.18	not detected
134459.45–001559.5	0.2448	2024	121	7.65	not detected
135943.14–003424.6	0.1630	2105	150	7.50	not detected
143704.12+000705.0	0.1403	1641	84	7.04	not detected
143847.54–000805.5	0.1040	4123	118	7.83	not detected
144930.49–004746.4	0.2532	8239	175	8.92	0.91
144932.70+002236.3	0.0806	882	83	6.47	not detected
145631.65–001114.2	0.1325	7542	118	8.40	not detected
151722.52–003002.8	0.4450	2085	172	8.15	not detected
151723.24–002709.3	0.1218	4376	188	8.02	0.89
151956.57+001614.6	0.1145	1537	103	6.99	not detected
152035.35–002040.1	0.1303	5788	138	8.32	not detected
152203.77+001128.3	0.2400	3012	221	8.00	not detected
152628.20–003809.4	0.1235	2203	87	7.48	0.65:
154344.28–001452.2	0.3018	2839	147	8.13	not detected
165338.68+634010.6	0.2793	1660	311	7.52	not detected

Table 1—Continued

SDSS J	z	FWHM _{Hβ} km s $^{-1}$	$\sigma_{\text{[OIII]}}$ km s $^{-1}$	$\log M_{\bullet}$ M_{\odot}	log R
165627.32+623226.9	0.1848	5271	191	8.42	not detected
165958.94+620218.1	0.2323	3919	169	8.17	not detected
170328.96+614109.9	0.0773	5480	196	8.18	not detected
170441.38+604430.4	0.3719	9504	167	9.92	2.15
171049.89+652102.1	0.3855	5098	386	8.72	not detected
171300.69+572530.3	0.3603	2660	352	8.06	0.65
171411.63+575834.0	0.0927	2129	180	7.53	not detected
171550.50+593548.8	0.0658	5326	121	8.47	not detected
171737.95+655939.3	0.2927	5017	290	8.66	not detected
171750.60+581514.1	0.3101	4092	253	8.50	not detected
171829.00+573422.4	0.1007	1388	205	7.09	not detected
171902.30+593715.9	0.1785	2086	124	7.53	not detected
172032.29+551330.2	0.2729	3604	138	8.16	not detected
172026.70+554024.2	0.3595	2777	177	8.33	not detected
172533.08+571645.6	0.0659	7480	109	8.25	not detected
172711.82+632241.9	0.2176	10535	169	9.18	not detected
173107.87+620026.1	0.0687	4863	164	8.19	not detected
173348.81+585651.0	0.4911	4277	202	8.71	not observed
232259.99–005359.4	0.1503	2617	213	7.85	0.20
232328.00+002032.9	0.1196	4320	150	8.18	not detected
233908.80–000637.8	0.4826	6795	242	9.10	not detected
234141.51–003806.7	0.3192	1820	175	7.75	0.44:
234932.77–003645.9	0.2790	3117	308	8.22	1.27:
235156.12–010913.4	0.1741	5332	175	8.72	2.48
235457.10+004219.9	0.2705	5721	440	8.61	not detected

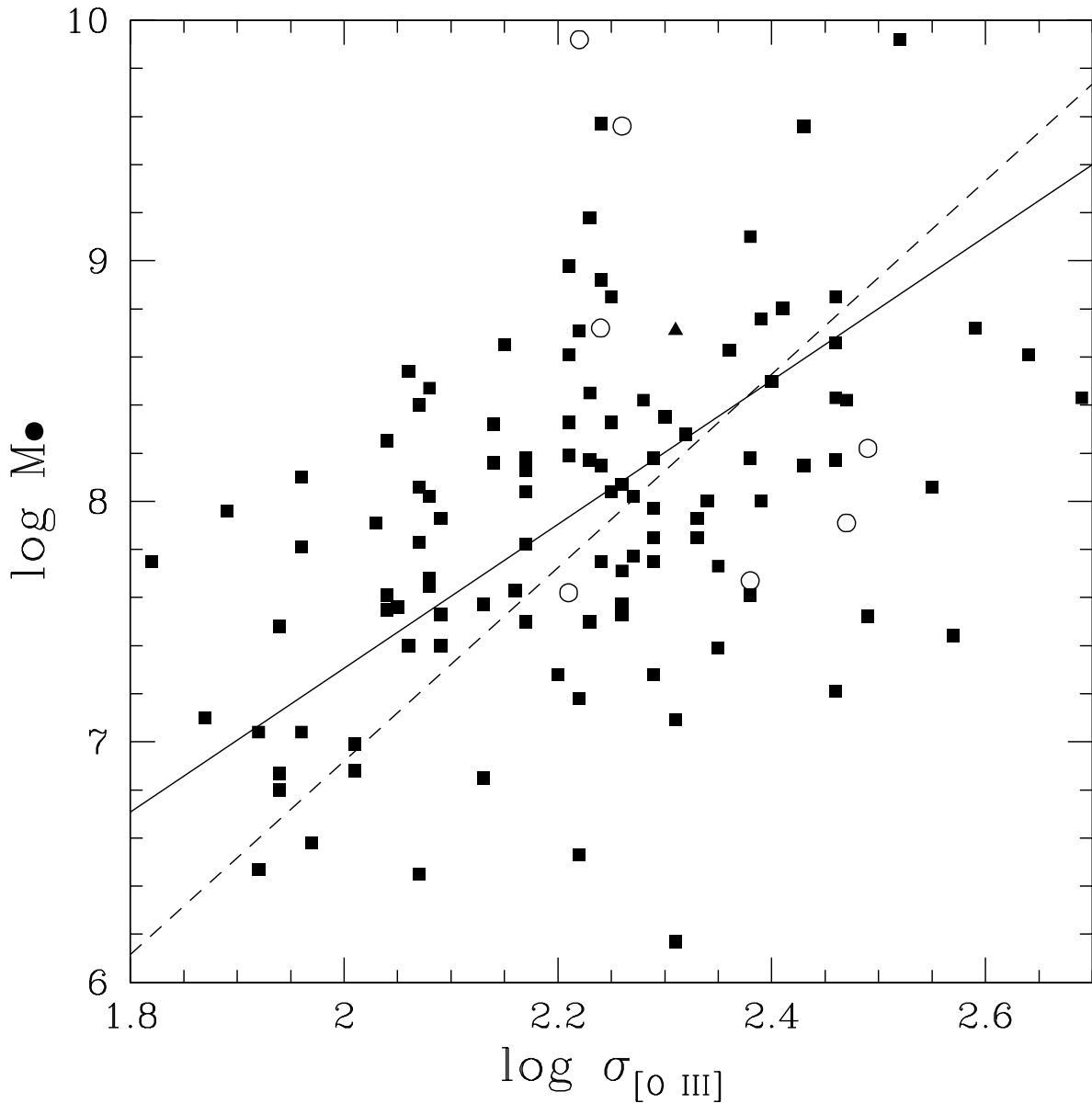


Fig. 1.— Log of the black hole mass in solar masses plotted against log of the velocity dispersion in km s^{-1} from the $[\text{O III}] \lambda 5007$ line. Radio quiet objects are shown as solid squares. Radio loud objects are shown as open circles. The single object unobserved in the radio is shown as an open triangle. The solid line is a bisector fit to the radio quiet points. The dashed line is the Tremaine et al. (2002) fit to nearby galaxies.

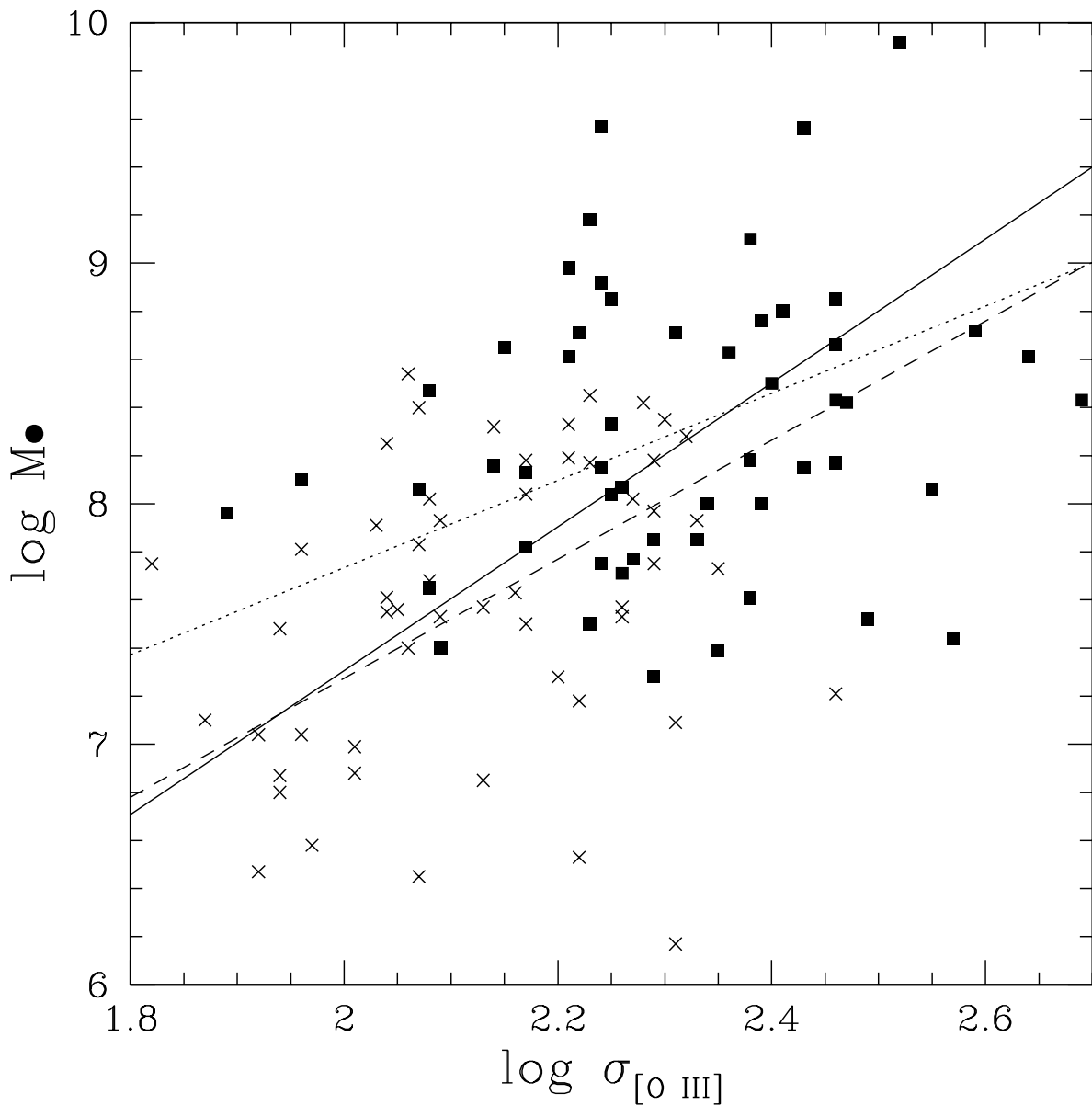


Fig. 2.— Same as Figure 1 but with radio-quiet objects divided into low (\times) and high (squares) luminosity subsamples. Fits are to (dashed) low luminosity, (dotted) high luminosity and (solid) whole sample.